ACS SENSORS

pubs.acs.org/acssensors

Article

Water-Selective Nanostructured Dehumidifiers for Molecular Sensing Spaces

Jiangyang Liu, Kazuki Nagashima,* Takuro Hosomi, Wenjin Lei, Guozhu Zhang, Tsunaki Takahashi, Xixi Zhao, Yosuke Hanai, Atsuo Nakao, Masaya Nakatani, Wataru Tanaka, Hikaru Saito, Masaki Kanai, Taisuke Shimada, Takao Yasui, Yoshinobu Baba, and Takeshi Yanagida*

Cite This: *ACS Sens.* 2022, 7, 534−544

Read Online

ACCESS | Metrics & More | Article Recommendations | Supporting Information

ABSTRACT: Humidity and moisture effects, frequently called water poisoning, in surroundings are inevitable for various molecular sensing devices, strongly affecting their sensing characteristics. Here, we demonstrate a water-selective nanostructured dehumidifier composed of $ZnO/TiO_2/CaCl_2$ core−shell heterostructured nanowires for molecular sensing spaces. The fabricated nanostructured dehumidifier is highly water-selective without detrimental adsorptions of various volatile organic compound molecules and can be repeatedly operated. The thermally controllable and reversible dehydration process of $CaCl_2{\cdot}nH_2O$ thin nanolayers on hydrophilic ZnO/TiO_2 nanowire surfaces plays a vital role in such water-selective and repeatable dehumidifying operations. Furthermore, the limitation of detection for sensing acetone and nonanal molecules in the presence of moisture (relative humidity ∼ 90%) was improved more than 20 times using nanocomposite sensors by operating the developed nanostructured dehumidifier. Thus, the proposed water-selective nanostructured dehumidifier offers a rational strategy and platform to overcome water poisoning issues for various molecular and gas sensors.

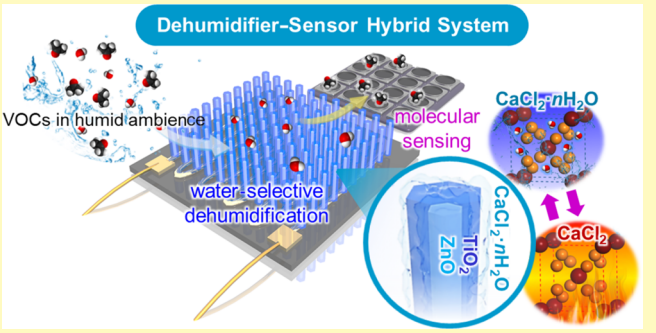

KEYWORDS: *nanostructured dehumidifier, $CaCl_2{\cdot}nH_2O$, nanowires, molecular and gas sensors, moisture effect*

The moisture effect is inevitable under atmospheric conditions and also well known to strongly affect and interfere with chemical events on various sensor surfaces and also their sensing performances, which is frequently called the "water poisoning effect".[1−5] This is mainly because water is a highly reactive chemical species, and the humidity value dynamically changes with the seasons and times of day.[6−9] In addition, a water vapor concentration for a typical relative humidity (RH) range (20−80%) is equivalent to 6000−25 000 parts per million (ppm) under 1 atm and 25 °C, which is clearly much higher than the conventional concentration range (from the parts per trillion to the ppm level) of volatile organic compound (VOC) analytes.[10,11] Thus, suppressing the moisture effect is strongly required for various sensors regardless of their sensing principles.[3,12−14] Substantial progress has been made through various approaches to suppress such water poisoning effects on sensor properties.[15−26] The most conventional approach is to adjust the sensing materials for reducing the moisture effect on sensing properties. This approach includes sensor surface decorations by hydrophobic additive, noble metal, and other materials.[18−26] For example, by introducing plasticizers to the polymer-based sensing film, the hydrophobicity of the polymer matrix can be enhanced, resulting in the immunity to humidity change.[18,19] Loading various metals, CuO and NiO as moisture absorbers on sensor surfaces, has also been intensively reported to suppress the moisture effect on sensing characteristics.[22−24] Another strategy is to employ multivalent metal cations on sensor surfaces, such as terbium (Tb), cerium (Ce), and praseodymium (Pr), since they are capable of acting as hydroxyl scavengers and going through regenerative self-refreshing without any electron transfers.[11,25,26] Although intensive efforts have been made via developing novel sensor materials and surfaces, it is still a challenging issue to fully suppress water poisoning effects under various sensing circumstances due to the limitation of material species usable for sensing.[27,28] The alternative interesting approach to overcome this water poisoning effect is to control the humidity of analyte vapor samples through pretreatment by desiccants.[2,29,30] A water filter/dehumidifier can be implemented prior to sensor spaces, controlling the humidity value. For example, Pratsinis et

Received: November 10, 2021
Accepted: January 12, 2022
Published: January 24, 2022

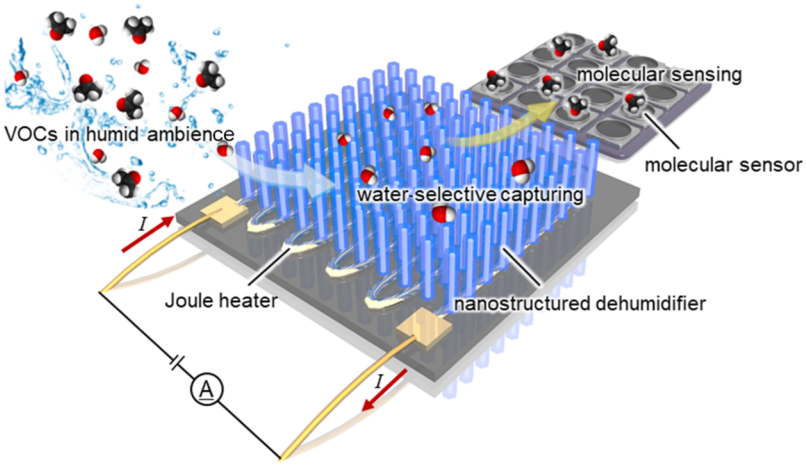

Figure 1. Schematic image of the proposed nanostructured dehumidifier composed of $ZnO/TiO_2/CaCl_2$ core−shell heterostructured nanowires for molecular sensors.

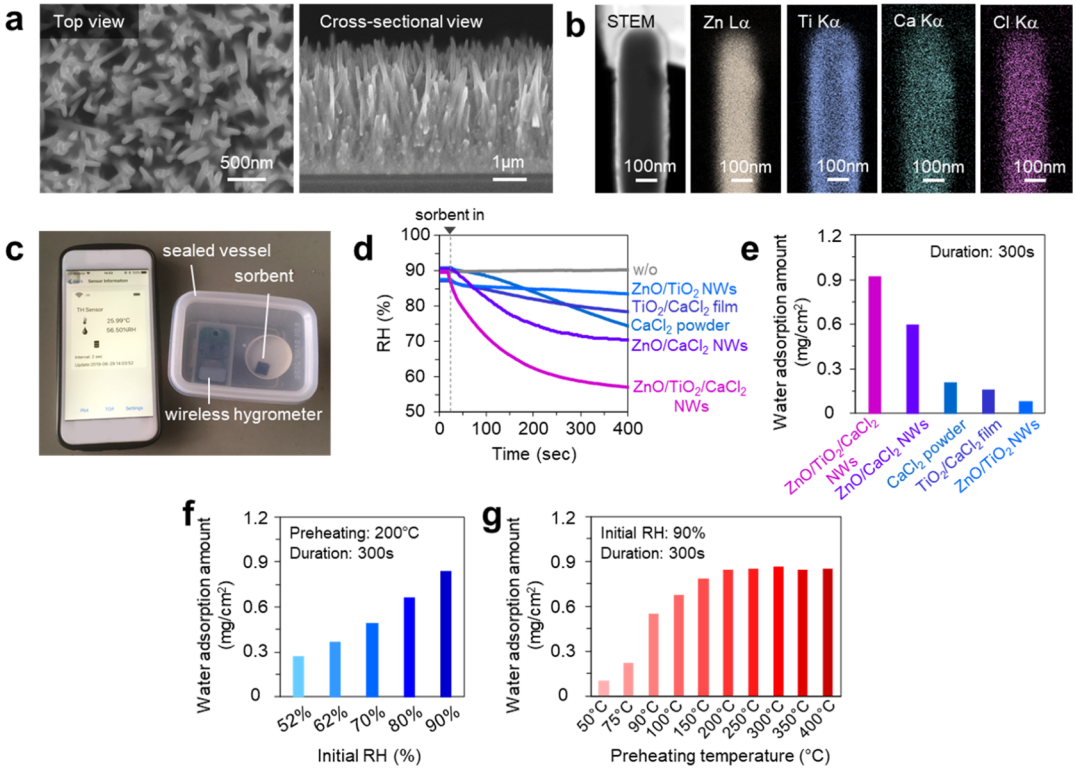

Figure 2. (a) SEM images of the fabricated $ZnO/TiO_2/CaCl_2$ core−shell heterostructured nanowires. (b) STEM images and EDS-based elemental mappings of the fabricated $ZnO/TiO_2/CaCl_2$ core−shell heterostructured nanowires. (c) Photographs of the measurement systems to examine the dehumidification ability. (d) Comparison between various water sorbents ($ZnO/TiO_2/CaCl_2$ core−shell heterostructured nanowires, $ZnO/CaCl_2$ core−shell heterostructured nanowires, ZnO/TiO_2 core−shell heterostructured nanowires, $CaCl_2$ powers (10 mg), and $TiO_2/CaCl_2$ thin films) on RH temporal changes, (e) Comparison of the water adsorption amount per surface area (mg/cm^2) data. (f) Effect of the initial RH values on the dehumidification ability of the nanostructured nanowires, and (g) preheating temperature effect on the dehumidification ability.

al. have proposed an interesting sensor system with filters composed of zeolite membranes or molecular separation columns to reduce the interference effect of water vapor and also other molecules for gas sensing.[31,32] Recently, a dehumidifier using a cold trap or dryer was developed to reduce the RH for detecting the analytes with high accuracy.[33,34] Although these previous studies have consistently utilized existing materials for their dehumidifying processes, there are several important issues in the developed dehumidifiers for sensor applications, including water selectivity during the drying process without detrimental loss of vapor analytes and a repeatability of dehumidifier operations.[35]

In this study, we propose a nanostructured dehumidifier for integrating with sensing devices to suppress water poisoning effects while maintaining intrinsic sensing properties. The required non-residual behavior of analyte molecules in dehumidifiers can be realized by utilizing an intrinsic water-selective nature of hydrated $CaCl_2 \cdot nH_2O$. A thermally controllable dehumidifying process is promising for water-selective and repeatable operations in a high humidity ambience. An

https://doi.org/10.1021/acssensors.1c02378
ACS Sens. 2022, 7, 534−544

integrated dehumidifier−sensor hybrid sensing device enables parts per billion-level molecular sensing even in high humidity surroundings.

RESULTS AND DISCUSSION

Figure 1 shows the schematic image of the proposed nanostructured dehumidifier composed of $ZnO/TiO_2/CaCl_2$ core−shell heterostructured nanowires for molecular sensors. This structure aims to control the humidity within a sensing space by placing water adsorption nanostructures (as a dehumidifier) near sensors. To prevent detrimental adsorptions of analytes, the nanostructures in devices must selectively adsorb water from the surroundings. For this purpose, we employed the nanostructures composed of $ZnO/TiO_2/CaCl_2$ core−shell heterostructured nanowires. The benefits of nanowire structures are an increase of surface area and also a spatial controllability of its crystal growth on a substrate.[36−38] The TiO_2 shell layer permanently retains the surface hydrophilicity to avoid detrimental aggregations of the hydrophilic $CaCl_2$ thin layer.[39] The effect of such a surface hydrophilicity will be discussed in a later section—Figure 3. The most outer $CaCl_2$ shell thin layer plays a role in adsorbing water within the sensing space. The reason why we employed $CaCl_2$ as the water-sorbent material is that $CaCl_2$ is well known to form hydrates $CaCl_2{\cdot}nH_2O$, which are stable enough under atmospheric environments.[40,41] Considering the nature of hydration in $CaCl_2{\cdot}nH_2O$ crystal structures,[42] the water-selective adsorption on the surface can be expected, although there have been no detailed investigations to examine such water absorption selectivity of $CaCl_2{\cdot}nH_2O$ crystal structures in the presence of VOCs. In addition, the number n of water molecules in $CaCl_2{\cdot}nH_2O$ crystal structures can be reversibly changed via controlling the surrounding humidity or temperature.[41,43] Thus, these inherent physical/chemical properties of $CaCl_2{\cdot}nH_2O$ crystal structures make $CaCl_2$ a promising candidate as a water-selective dehumidifier material in the proposed device structure.

Figure 2a,b shows the scanning electron microscopy (SEM) images and scanning transmission electron microscopy (STEM) images with energy-dispersive X-ray spectroscopy (EDS) of fabricated $ZnO/TiO_2/CaCl_2$ core−shell heterostructured nanowires. A hydroxyl-rich TiO_2 shell layer (thickness-19 nm) was synthesized using the atomic layer deposition (ALD) method onto hydrothermally grown ZnO nanowires. The TiO_2 surface hydrophilicity facilitates the later spin-coating process of $CaCl_2$ and also prevents detrimental aggregations of the hydrophilic $CaCl_2$ thin layer (thickness 4−20 nm). The details of fabrication procedures can be seen in the Experimental Section and Supporting Information (Figures S1−S5). As seen in Figure 2a,b, the nanowire morphology can be maintained during shell-layer formations, and the uniform shell-layer coating can also be seen in these images. Figure 2c shows the photographs of the measurement system to examine the dehumidification ability of the fabricated $ZnO/TiO_2/CaCl_2$ core−shell heterostructured nanowires, which is placed in a confined vessel (volume: 140 cm^3) with a wireless hygrometer. The nanostructures were preheated at 200 °C for 3 min using a hotplate to be dehydrated. Then, the samples were immediately transferred into the confined vessel with the desired humid atmosphere, which was controlled by flowing humid air into the vessel at room temperature (RT), and the detailed information can be seen in the Experimental Section. It is noted that during the hygroscopic operation, the vessel was sealed. Figure 2d shows the measured RH data as a function of dehumidifying time for cases when introducing the synthesized sorbents. In the presence of a nanostructured $ZnO/TiO_2/CaCl_2$ dehumidifier, the RH value most significantly decreased from 90% down to 57% within 400 s when compared with other sorbents under the same preheating conditions, highlighting the significant dehumidifying effect by introducing a $CaCl_2$ layer onto nanowire surfaces. By measuring the variation of the RH value during the dehumidifying process, we calculated the amount of adsorbed water molecules per surface area, as shown in Figure 2e. The effect of the initial RH values on the dehumidification ability of fabricated nanostructures is also examined, as shown in Figure 2f. The data when preheating at 200 °C for 3 min and dehumidifying for 300 s of duration time are shown. Clearly, the dehumidification effect of the fabricated nanostructures tends to enhance with increasing initial RH values. This enhanced trend in dehumidification was also observed when increasing the chamber volume with the same initial RH (Figure S6). The fabricated dehumidifier can be operated down to the initial RH value of approx. 35% (Figure S6) for the present dehumidifying test configurations. In addition, we examine the effect of preheating temperatures on the dehumidification ability of the fabricated nanostructures, as shown in Figure 2g. The data when dehumidifying for 300 s of duration time and the initial RH value of 90% are shown. The dehumidification effect (*i.e.*, the amount of adsorbed water molecules) tends to increase on increasing the preheating temperature from 50 °C up to 200 °C, and then it is almost saturated above 200 °C. These results demonstrate the significant effect of preheating temperatures on the dehumidification effect of fabricated nanostructures. Furthermore, as shown in Figure 3, the dehumidification effect is highly repeatable when cycling heating and cooling processes under atmospheric environments. During these thermal cycling processes, there is a significant effect of the surface hydrophilicity on the morphology and the dehumidification ability. As shown in Figure 3, the cycling endurance of the dehumidification ability is high when employing $ZnO/TiO_2/CaCl_2$ core−shell heterostructured nanowires. On the other hand, such good cycling endurance was no longer observable for $ZnO/CaCl_2$ core−shell heterostructured nanowires, highlighting the significant role of a hydrophilic TiO_2 layer on the dehumidifying endurance ability. SEM−EDS images and wetness test data of Figure 3a,b reveal the importance of the surface hydrophilicity to maintain a thin hydrophilic $CaCl_2$ layer without detrimental aggregations (Figure S7). Thus, the above results highlight that fabricated $ZnO/TiO_2/CaCl_2$ core−shell heterostructured nanowires are capable of repeated dehumidification of sensing spaces.

Hydration/dehydration processes of $CaCl_2{\cdot}nH_2O$ must correlate with the observed experimental trends in Figures 2 and 3. When preheating the nanostructures at relatively higher temperatures, the dehydration process on the surface proceeds, and the n value of $CaCl_2{\cdot}nH_2O$ tends to be lower than those when preheating at higher temperatures.[41,43] A vacancy of water coordination sites in $CaCl_2{\cdot}nH_2O$ might enhance the observed dehumidification effect. In order to more directly reveal the above speculated dehydration/hydration behaviors on the surfaces of $ZnO/TiO_2/CaCl_2$ core−shell heterostructured nanowires, we performed Fourier transform infrared (FT-IR) spectroscopy measurements when varying preheating temperatures ranged from RT up to 400 °C, as shown in Figure 4a. The data for the scissor bend band at 1550−1750 cm^{-1} and symmetric and asymmetric stretch bands at 2800−4000 cm^{-1} of H_2O are shown in the figure. In the temperature range below 70 °C, the features of the spectra are well consistent with those of

https://doi.org/10.1021/acssensors.1c02378
ACS Sens. 2022, 7, 534−544

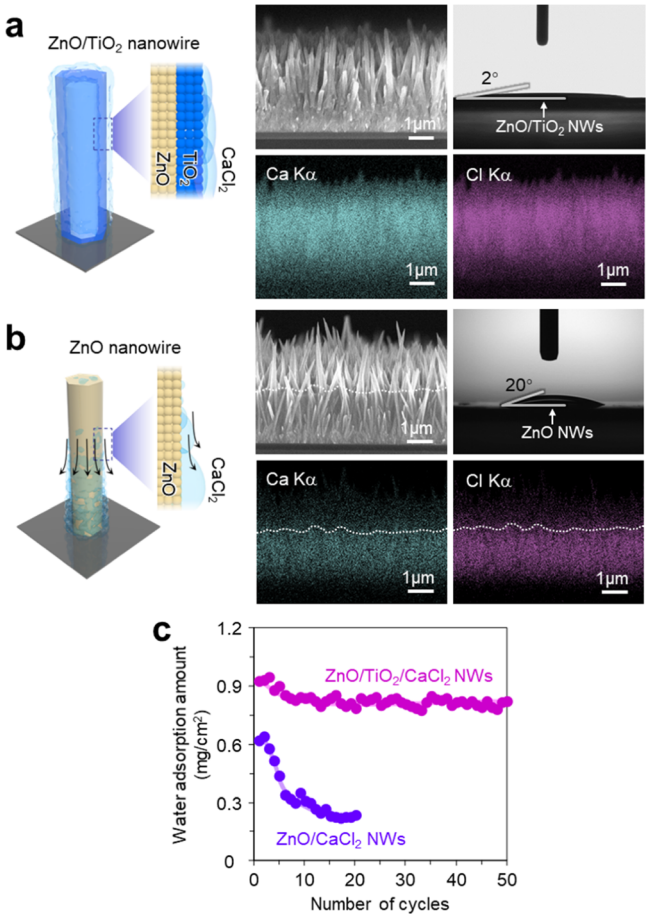

Figure 3. (a) Schematic illustration, SEM−EDS images, and snapshot of the water contact angle measurement of the $ZnO/TiO_2/CaCl_2$ core−shell heterostructured nanowires. (b) Schematic illustration, SEM−EDS images, and snapshot of the water contact angle measurement of the $ZnO/CaCl_2$ core−shell heterostructured nanowires. (c) Endurance data of cycling dehumidifying processes on the water adsorption amount of the $ZnO/TiO_2/CaCl_2$ core−shell heterostructured nanowires and the $ZnO/CaCl_2$ core−shell heterostructured nanowires.

water molecules on the surface (Figure S8).[44] Above 70 °C, the data tend to exhibit the spectra assigned to hydrates $CaCl_2 \cdot nH_2O$ (n = 6, 4, 2),[43] and n values tend to decrease with increasing temperatures. These temperature ranges for hydrates $CaCl_2 \cdot nH_2O$ (n = 6, 4, 2) agree with previous reports.[43,45,46] These spectroscopic trends highlight that a dehydration process in the fabricated $ZnO/TiO_2/CaCl_2$ core−shell heterostructured nanowires occurs with increasing temperatures. From the repeatable dehumidification performance in Figure 3, the hydration/dehydration processes of $CaCl_2 \cdot nH_2O$ are also expected to be reversible. Figure 4b−e shows the schematic and FT-IR data when cycling the heating/cooling process when varying the temperatures ranging between RT and 200 °C. Clearly, the hydration/dehydration processes in the FT-IR data are reversible, which is consistent with the results in Figure 3. Thus, these results reveal that reversible hydration/dehydration processes of $CaCl_2 \cdot nH_2O$ play an essential role in the repeatable dehumidifying/humidifying data in Figure 3.

Next, we examine the water-selective adsorption on the fabricated $ZnO/TiO_2/CaCl_2$ core−shell heterostructured nanowires with the coexistence of analytes (VOC molecules: ethanol, acetone, nonane, 2-nonanone, and 1-nonanal), as illustrated in Figure 5a. Figure 5b shows the adsorbed amount ratio of molecules to water during the dehumidifying operation with the initial RH value of 87% and the preheated temperature of 200 °C. The adsorbed amounts of analytes were measured by using gas chromatography−mass spectrometry (GC−MS). The details can be seen in the Experimental Section and Supporting Information (Figures S9 and S10). As seen in Figure 5b, the fabricated nanostructures selectively adsorb water molecules even with the coexistence of analytes. Note that the adsorbed amount of water was 10 000 times larger than those of other analyte VOC molecules. The adsorbed amounts of VOCs are rather low; among the present analytes, the order of the highest adsorbed amount is ethanol > nonanal > 2-nonanone ∼ acetone > nonane, which is almost consistent with the degree of their hydrophilicity. Even varying the dehumidifying conditions (the initial RH value, preheated temperature, and the CO_2 content) as shown in Figures 5c,d and S11, the superior water-selective adsorption on the fabricated $ZnO/TiO_2/CaCl_2$ core−shell heterostructured nanowires can be almost maintained. Although the adsorbed amount of analytes slightly increases with the decreasing initial RH value and increasing preheating temperatures, the water selectivity of the adsorption behaviors on $CaCl_2 \cdot nH_2O$ surfaces is still significant. Thus, these results highlight the superior water selectivity of the present $ZnO/TiO_2/CaCl_2$ core−shell heterostructured nanowire dehumidifier even with the coexistence of analytes.

Figure 6a,b shows a comparison of both the dehumidifying speed and the adsorbed water amount, revealing the superior dehumidifying ability of the present nanostructured dehumidifier compared to that of the conventional molecular sieve. Furthermore, Figure 6c,d shows the water adsorption selectivity against analytes, shown as the adsorbed molecular percentage in the figures, highlighting also the superior water adsorption selectivity of the present nanostructured materials. These advantages are because the present nanostructured dehumidifier utilizes their surface rather than inside pores (used in a molecular sieve), and the surface nature of $CaCl_2 \cdot nH_2O$ indicates the higher water selectivity (Figure S12). Finally, we examine the application of the proposed dehumidifier to suppress water poisoning effects for gas sensors. Figure 7a−c shows the schematic image, the photographs, and the thermal images of the fabricated nanostructured dehumidifier−sensor hybrid systems. The employed chamber volume is designed to be 216.5 mm^3. The details of the employed sensor can be seen elsewhere (Figure S13).[47,48] The nanostructured dehumidifier can be heated up by an S-shaped Pt micro-heater on the substrate, as seen in Figure 7b,c. We confirmed that applying the electrical voltage of 13 V to the micro-heater increases the temperature of the dehumidifier up to 188 °C during the humid gas flow period of 1 min (see the temperature curve data in Supporting Information Figure S14). Figure 7a shows the illustration of the operated gas flow and the corresponding monitored sensor response experimental data in humid air together with 2.8 ppm humid acetone (RH ∼ 90%), respectively. The detailed experimental procedures can be seen in the Experimental Section. As can be seen in Figure 7d, when introducing humid gas with the analyte (acetone), the employed sensor quickly responds. When starting the dehumidifying process by tuning off the heater, there is a difference in the resistance values (ΔS) between the two data with and without the analyte. The extracted ΔS values for two analytes (acetone and nonanal) were shown as a function of the nominal concentration of target analytes, as shown in Figure 7e,f. Clearly,

https://doi.org/10.1021/acssensors.1c02378
ACS Sens. 2022, 7, 534−544

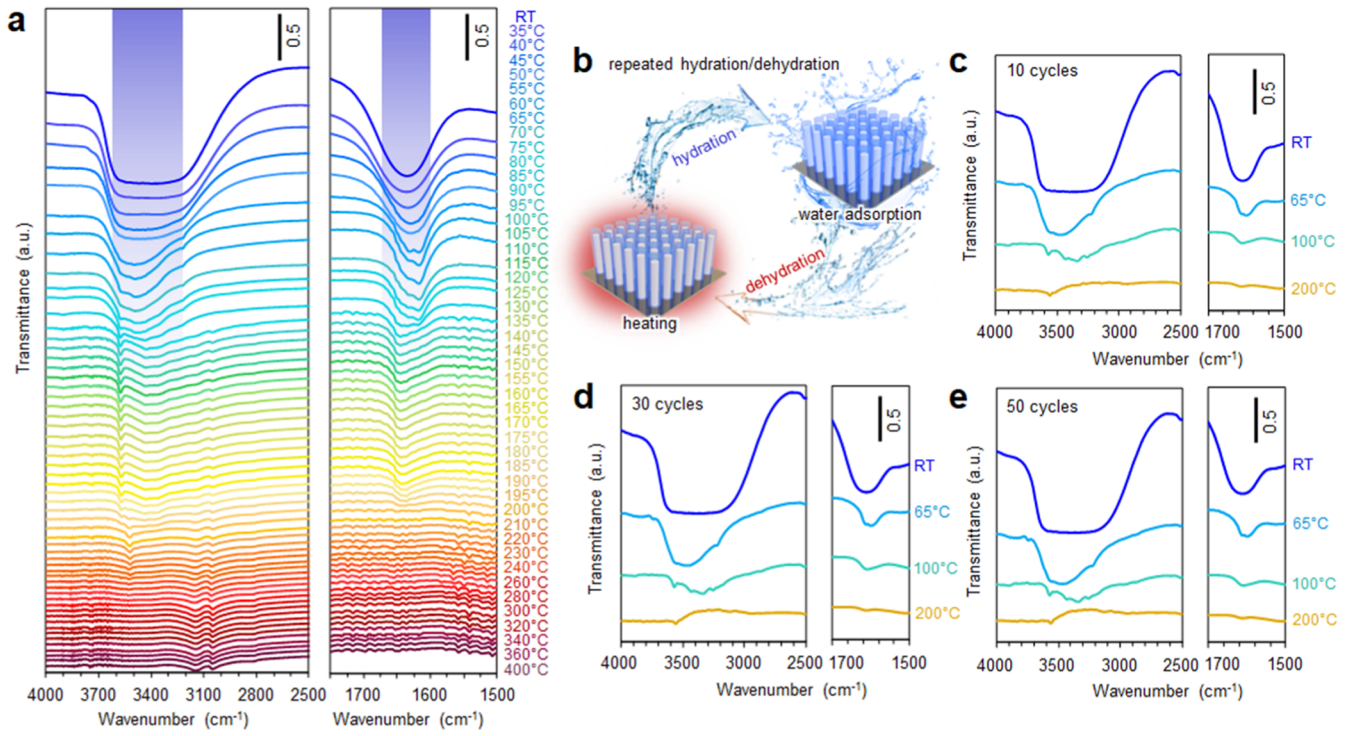

Figure 4. (a) Temperature-dependent FT-IR spectroscopy data of water molecules on the $ZnO/TiO_2/CaCl_2$ core−shell heterostructured nanowires. (b) Schematic illustration and (c−e) FT-IR data of the $ZnO/TiO_2/CaCl_2$ core−shell heterostructured nanowires during the dehydration/hydration cycling process (shown by the 10th cycle, 30th cycle, and 50th cycle spectra, respectively).

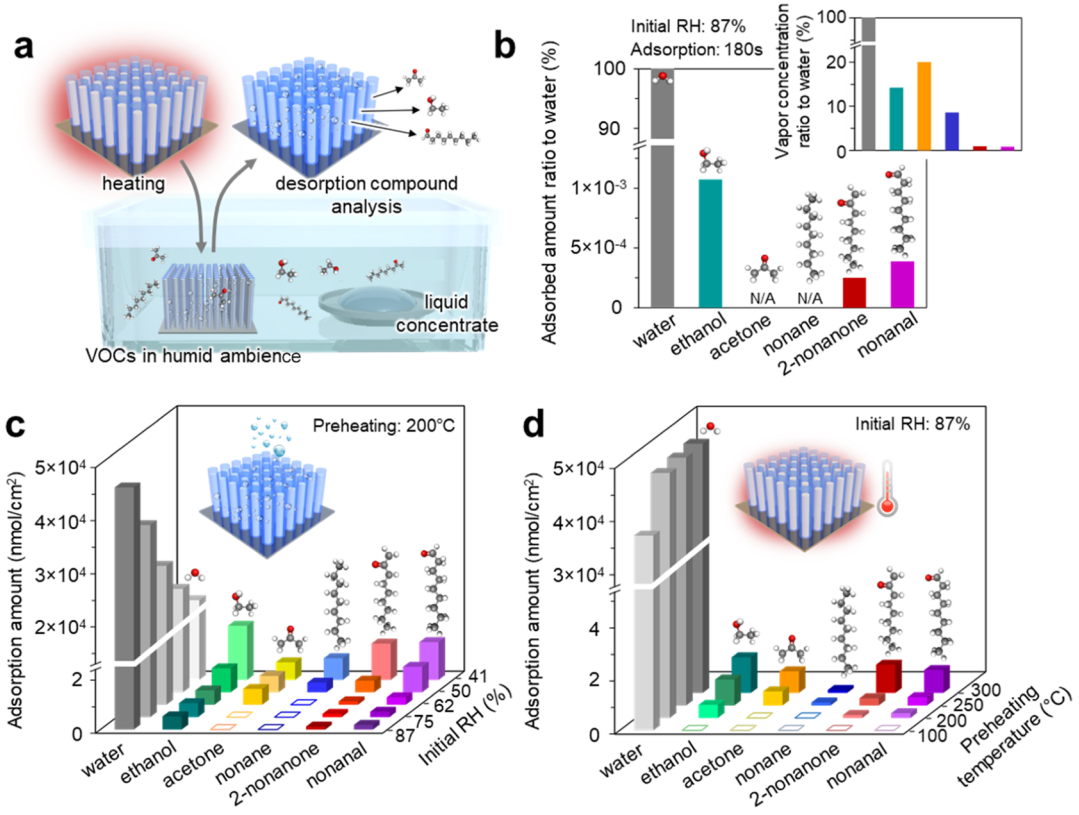

Figure 5. (a) Schematic illustration of molecular adsorption measurements for the fabricated nanostructured dehumidifier in a humid ambience. (b) Adsorption amount ratio of VOCs (ethanol, acetone, nonane, 2-nonanone, and nonanal) to water when employing the $ZnO/TiO_2/CaCl_2$ core−shell heterostructured nanowires. The inset shows the vapor concentration ratio of VOCs to water. (c) Effect of initial RH values on adsorption amount data for water and VOCs when employing the $ZnO/TiO_2/CaCl_2$ core−shell heterostructured nanowires. (d) Effect of preheating temperatures on the adsorption amount (per cm^2 substrate) data for water and VOCs when employing the $ZnO/TiO_2/CaCl_2$ core−shell heterostructured nanowires.

https://doi.org/10.1021/acssensors.1c02378
ACS Sens. 2022, 7, 534−544

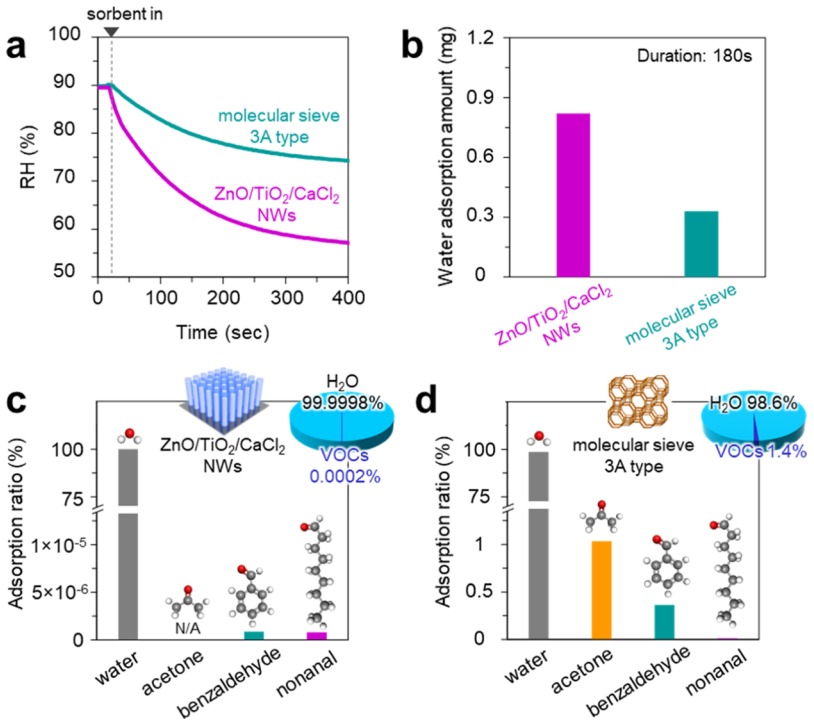

Figure 6. (a) Comparison between the effects of the $ZnO/TiO_2/CaCl_2$ core−shell heterostructured nanowires and the molecular sieve (10 mg, zeolite, 3A type) on RH temporal changes during the dehumidifying process. (b) Comparison of water adsorption amount data at 180 s of the duration time. (c) Adsorption amount data of the $ZnO/TiO_2/CaCl_2$ core−shell heterostructured nanowires for water and VOCs (acetone, benzaldehyde, and nonanal). (d) Adsorption amount data of the molecular sieve for water and VOCs (acetone, benzaldehyde, and nonanal).

the limit of detection (LOD) is significantly lowered by operating the present nanostructured dehumidifier for both analytes (the details are shown in Figures S15−S17). The LOD values (as listed in Table 1) for acetone and nonanal improve 23 times and 20 times, respectively. Thus, employing the proposed nanostructured dehumidifier sufficiently enhances the sensor performance under high humidity conditions, where there has been a strong restriction of usable sensor materials and systems. Since, in principle, the proposed approach can be applied for almost any sensor system, the implications in this work would be a foundation to tackle one of the serious sensor issues—the water poisoning effect.

CONCLUSIONS

In summary, we propose a water-selective nanostructured dehumidifier composed of $ZnO/TiO_2/CaCl_2$ core−shell heterostructured nanowires for molecular sensors. The proposed nanostructured dehumidifier is highly water-selective and can be repeatedly operated to suppress moisture effects for sensing various VOC molecules under high humidity conditions. A thermally controllable dehydration process of $CaCl_2 \cdot nH_2O$ on hydrophilic ZnO/TiO_2 nanowire surfaces plays a vital role in such water-selective and repeatable operations. Furthermore, the molecular (acetone and nonanal) sensing limitation in the presence of moisture (RH ∼ 90%) was greatly improved (more than 20 times) when operating the developed nanostructured dehumidifier. Thus, the present nanostructured dehumidifier offers a rational strategy to overcome water poisoning issues in various molecular and gas sensors for reliable data collection.

EXPERIMENTAL SECTION

Preparation of $ZnO/TiO_2/CaCl_2$ Nanowires. ZnO nanowires were grown on a 100 nm-thick SiO_2-coated Si(100) substrate by a seed-assisted hydrothermal synthesis.[49−53] First, a 30 nm-thick ZnO seed layer was deposited on a substrate with a 1 nm-thick Ti adhesion layer by radio frequency (RF) sputtering at an RF power of 50 W and an Ar pressure of 0.3 Pa. The substrate was immersed into a 150 mL aqueous solution containing 25 mM zinc nitrate hexahydrate $(Zn(NO_3)_2 \cdot 6H_2O$, Wako 99.0%), 25 mM hexamethylenetetramine $[(CH_2)_6N_4$, Wako 99.0%], and 2.5 mM polyethyleneimine (number average mw 1800, Aldrich 50 wt % in H_2O). The hydrothermal growth of ZnO nanowires was conducted at 95 °C for 12 h in an oven. After the growth, the samples were taken out from the aqueous solution, rinsed in deionized (DI) water, and dried by air blowing. To remove the organic residuals on the ZnO nanowires, an oxygen plasma treatment was performed at 150 W in a 1 Torr oxygen atmosphere for 10 min. A hydrophilic TiO_2 layer with a thickness of ca. 15 nm was then deposited on the ZnO nanowires by using ALD (Ultratech, Savannah S100) at 150 °C with tetrakis(dimethylamido)titanium ($Ti(NMe_2)_4$) as a precursor. Finally, a $CaCl_2$ layer was deposited on the ZnO/TiO_2 nanowires. A $CaCl_2$-containing aqueous solution was prepared by dissolving $CaCl_2$ powder (Wako 99.0%) into DI water with controlling the concentration in the range of 1−5 M. 50 μL of the prepared solution was dropped and spin-coated on the ZnO/TiO_2 nanowires at a rotation speed of 4000 rpm for 1 min. Subsequently, the sample was baked for 3 min on a hotplate with varying the temperature in the range of 50−400 °C to dehydrate $CaCl_2$. As control samples, ZnO nanowires, ZnO/TiO_2 nanowires, and $ZnO/CaCl_2$ nanowires were prepared, and the dehumidification performance was evaluated together with the $ZnO/TiO_2/CaCl_2$ nanowires.

Characterization of $ZnO/TiO_2/CaCl_2$ Nanowires. A scanning electron microscope (JEOL JSM-7610F) equipped with an energy-dispersive X-ray spectroscope was used to characterize the morphology and the composition of the fabricated nanowires. The accelerating voltages used in the SEM−EDS analyses were 15 kV for the nanowires on a substrate and 30 kV for the single nanowire, respectively. A Fourier transform infrared spectroscope (Thermo Fisher Scientific Nicolet

https://doi.org/10.1021/acssensors.1c02378
ACS Sens. 2022, 7, 534−544

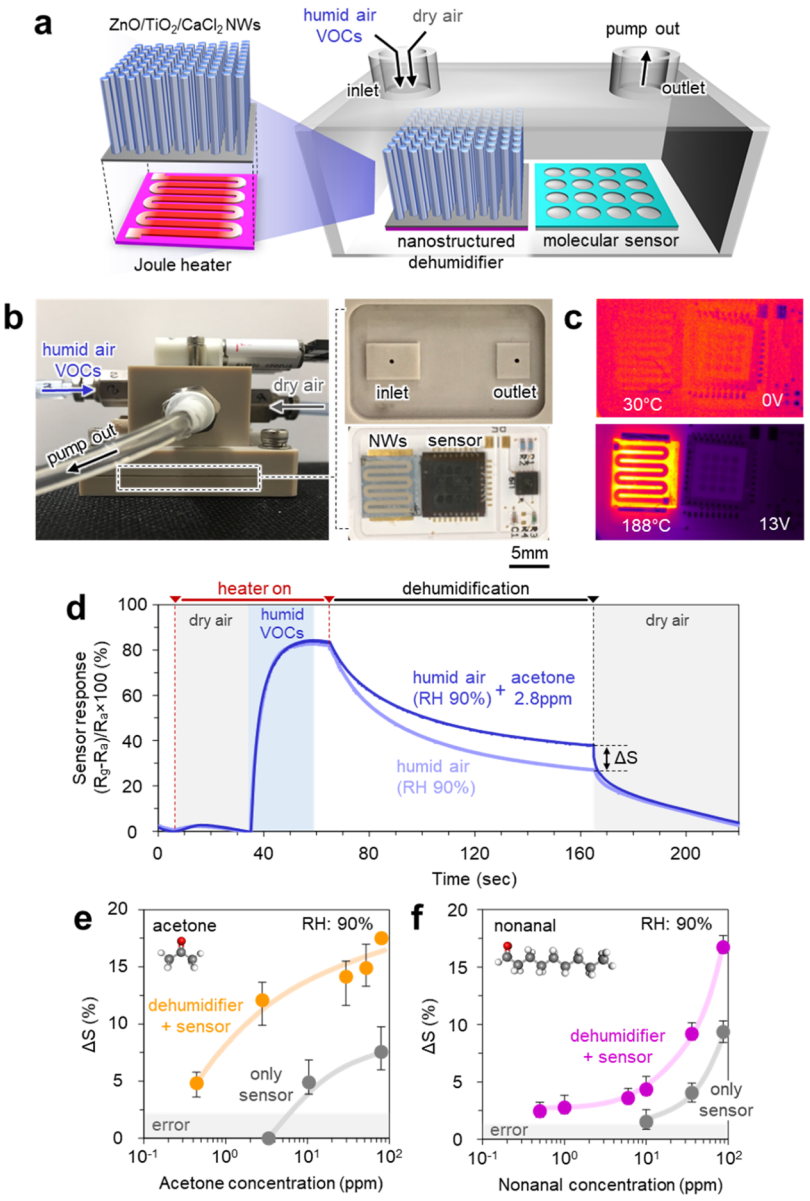

Figure 7. (a) Schematic illustration and (b) photographs of the nanostructured dehumidifier−sensor hybrid system. (c) Thermal images when applying an electrical voltage of 13 V to the micro-heater. (d) Sensor response data as a function of the operating time and the effect of VOCs on the sensor response. Sensing responses to (e) acetone and (f) nonanal obtained by the hybrid sensing platform in an RH ∼ 90% humid atmosphere. As controls, sensing responses without the dehumidifier are also shown.

Table 1. LOD for VOCs (Acetone and Nonanal) Sensing in the Dehumidifier−Sensor Hybrid System and Only a Sensor[a]

analyte VOCs	LOD dehumidifier + sensor (ppm)	LOD only sensor (ppm)	LOD ratio
acetone	0.4	10.4	23 times
nonanal	0.5	10.0	20 times

[a]LOD ratio between two sensing systems is also shown.

iS50) equipped with an MCT (HgCdTe) detector was used to evaluate the adsorption status of water on the nanowires and the $CaCl_2$ powder. For the temperature dependence, the samples were heated to the given temperature, kept for 5 min, and measured in the range of 800−4000 cm^{-1} with a resolution of 4 cm^{-1}.

Evaluation of the Dehumidification Performance of the Sorbents. In order to evaluate the dehumidification performance of the sorbents, a confined vessel was filled with humid air and the RH value in the vessel was monitored by a wireless hygrometer (Uni-Electronics, Logtta UNI-01-B002) when introducing a sorbent into the vessel. The humid air was generated by a humidity controlling system (KOFLOC, WMG-10) in the range of 35−90% and allowed to flow in the vessel. Then, the vessel was sealed and kept for 1 min until the RH value became stable. A sorbent preheated for 3 min was immediately introduced into the vessel and the variation of RH value was monitored. The sample size was 10 mm × 10 mm. The vessel volume and the preheating temperature were varied in the range of 140−700 mL and 50−400 °C, respectively. In this measurement, the dehumidification performances of ZnO nanowires, ZnO/TiO_2 nanowires, $ZnO/CaCl_2$ nanowires, and $ZnO/TiO_2/CaCl_2$ nanowires were evaluated. As control samples, 10 mg of $CaCl_2$ powder and 10 mg of a molecular sieve (3A type) were also employed. The water adsorption amount M_{water} is calculated by the following equation: $M_{water} = \Delta RH \times S \times V_{vessel}$, where ΔRH is the change of the RH value during the measurement, S is the saturated humidity value at a given pressure and temperature, and V_{vessel} is the vessel volume. In this study, $S = 22.8$ g/m^3 under the condition of atmospheric pressure (101 kPa) and RT (25 °C) was used.

https://doi.org/10.1021/acssensors.1c02378
ACS Sens. 2022, 7, 534−544

Molecular Adsorption Property of ZnO/TiO_2/$CaCl_2$ Nanowires. The molecular adsorption property of the ZnO/TiO_2/$CaCl_2$ nanowires was evaluated by analyzing their desorbed compounds using a gas chromatograph−mass spectrometer (SHIMADZU GCMS-QP2020 Ultra). First, the RH-controlled humid air was allowed to flow into a 25 mL vial bottle, and 2 μL of the liquid concentrate of each analyte molecule was dropped at the bottom of the vial bottle. The vial bottle was sealed and kept for 30 min to vaporize the analyte molecules. The samples of ZnO/TiO_2/$CaCl_2$ nanowires cut into a size of 2 mm × 20 mm were used. The samples were preheated on a hotplate in the range of 100−300 °C for 3 min. The suspended samples were inserted in the vial bottle filled with analyte vapor molecules and kept for 3 min. Then, the samples were transferred to the gas chromatograph−mass spectrometer for analyzing the desorbed compounds. The desorbed compounds' analysis was performed using the gas chromatograph−mass spectrometer equipped with an inlet temperature control unit (OPTIC4) and a capillary column (GL Science InertCap, FFAP). For the desorption, the inlet temperature of 300 °C was used. As a control sample, 10 mg of the molecular sieve (3A type) was also employed. The amount of each desorbed compound was estimated by making calibration curves.

Computational Details. The adsorption energy of acetone on $CaCl_2 \cdot nH_2O$ was estimated by the first principle calculation based on density functional theory using the DMol^3 module of the Materials Studio (2017). The simulation was performed by combining the semilocal generalized gradient approximation with the Perdew−Burke−Ernzerhof exchange−correlation function. The equilibrium crystal structures of $CaCl_2 \cdot nH_2O$ were obtained via geometry optimization in the Broyden−Fletcher−Goldfarb−Shanno minimization scheme. In the geometry optimization, the criteria of convergence were set to be 1.0×10^{-5} eV/atom for energy, 0.03 eV/Å for force, 1×10^{-3} Å for ionic displacement, and 0.05 GPa for stress, respectively. For the force field, the COMPASS energy setting was employed in this study. The employed parameters were carefully tested for converging the total energy.

Nanostructured Dehumidifier−Sensor Hybrid Systems and Molecular Sensing Measurement. A nanostructured dehumidifier−sensor hybrid system was fabricated to evaluate the effect of water-selective dehumidification of ZnO/TiO_2/$CaCl_2$ nanowires on the molecular sensing performance. The nanostructured dehumidifier device was fabricated on a 100 nm-thick SiO_2-coated Si substrate. First, an S-shaped Pt micro-heater was fabricated on the substrate by using RF sputtering with a metal mask at an RF power of 50 W and an Ar pressure of 0.3 Pa. The thickness of the Pt micro-heater was 100 nm. A 1 nm-thick Ti was used as an adhesive layer. Then, the ZnO/TiO_2/$CaCl_2$ nanowires were grown on the micro-heater. The samples were cut into a size of 6 mm × 7 mm. For the sensor device, a polymer−carbon black nanocomposite was first prepared by mixing carbon black (CB2350, Mitsubishi Chemical) and polyethylene glycol (PEG) (PEG4000, Aldrich Chemical Co.) in DI water at the concentrations of 10 mg/mL for each material. The nanocomposite was then deposited on a 100 nm-thick SiO_2-coated Si substrate. Prior to the deposition of the nanocomposite, the comb-shaped Pt electrodes with a Ti adhesive layer were patterned on a 7 × 7 mm^2-sized substrate by combining photolithography and RF sputtering. The gap distance and the thickness of the Pt electrodes were 40 μm and 400 nm, respectively. A SU-8 photoresist layer with a 45 μm thickness was coated on the electrode-patterned substrate by spin-coating, and circular hole patterns were formed on the SU-8 layer by photolithography. The PEG−carbon black mixed solution was dropped on the patterned substrate by the ink-jet printing technique (custom-made, SIJ Technology Inc.). The sensor device was finally obtained by performing vacuum annealing at 120 °C for 24 h to fully remove the solvent. The nanostructured dehumidifier device and the sensor device were integrated on a printed circuit board (PCB) in a side-by-side manner. The electrical connections between the devices and the PCB were made by Au wires using a wire bonder. The performance of the Pt micro-heater for the dehumidifier device was evaluated by using a thermo camera (InfraTec, VarioCAM) by varying the applied voltage. For the molecular sensing measurement, the sensing chamber was created by polyether ether ketone with a chamber volume of 216.5 mm^3. The sensing chamber was equipped with solenoid valves and a hand-top air pump. For the measurement, humid air with analyte molecules (humid gas) and dry air were collected using 20 L of the sampling bags (GL Sciences, ANALYTIC-BARRIER AB-20L 3008-99320) and sequentially allowed to flow into the sensing chamber for introducing and flushing the analyte molecules, respectively. As the analyte molecules, acetone and nonanal were employed in this study. The concentration of analyte molecules in the sampling bag was validated by GC−MS. The electrical sensing response of the sensor devices was measured by a homemade sensing module at RT with a readout voltage of 1 V. The workflow of the molecular sensing measurement is as follows. First, the dry air was allowed to flow into the chamber, and the dehumidifier device was heated up for dehydration. Then, dry air was switched to humid gas. After filling the sensing chamber with humid gas, the solenoid valve was closed to seal the chamber, and the micro-heater was turned off for starting the dehumidification of the sensing chamber. This condition was kept for 3 min. Finally, dry air was allowed to flow into the chamber for flushing the humid gas. The sensor response ΔR is defined as $\Delta R = (R_g - R_a)/R_a \times 100\%$, where R_g and R_a are the sensor resistances under humid gas flow and dry air flow, respectively. The sensor response to an analyte molecule ΔS was estimated by subtracting the sensor response to humid air $\Delta R_{\text{humid-air}}$ (without analyte molecules) from that to humid gas $\Delta R_{\text{humid-gas}}$ (with analyte molecules), that is, $\Delta S = \Delta R_{\text{humid-gas}} - \Delta R_{\text{humid-air}}$. The error response from the background humid air was determined by carefully checking the variation of the sensor response to humid air.

■ ASSOCIATED CONTENT

Supporting Information

The Supporting Information is available free of charge at https://pubs.acs.org/doi/10.1021/acssensors.1c02378.

Schematic illustrations of the heterostructured ZnO/TiO_2/$CaCl_2$ fabrication process, optimization of the ZnO/TiO_2/$CaCl_2$ nanowire fabrication process, illumination of the importance of the TiO_2 inter-layer, demonstration of core−shell heterostructure nanowires by TEM images, evaluation of the thickness of the $CaCl_2$ out-layer, dehumidifying property of the heterostructured ZnO/TiO_2/$CaCl_2$ nanowire, space dehumidification by $CaCl_2$ powder, FT-IR spectra of the $CaCl_2$ powder and ZnO/TiO_2 heterostructured nanowires, molecular adsorption amount evaluation and calibration, schematic illustration of vapor component analysis, effect of CO_2 on the adsorption amount of water and VOCs by the ZnO/TiO_2/$CaCl_2$ nanowire, computational simulation of molecular adsorption on $CaCl_2 \cdot nH_2O$, optical microscopy of the PEG−carbon black nanocomposite sensor and SEM images of the sensing material, temperature profiles of the nanostructured dehumidifier and sensor, sensor responses to humid gas and humid air via a sensor without a dehumidifier, sensor responses to humid gas (acetone) and humid air with an RH value of 90% via a dehumidifier sensor hybrid system, and sensor responses to humid gas (nonanal) and humid air with an RH value of 90% via a dehumidifier−sensor hybrid system (PDF)

■ AUTHOR INFORMATION

Corresponding Authors

Kazuki Nagashima − *Department of Applied Chemistry, Graduate School of Engineering, The University of Tokyo, Tokyo 113-8656, Japan; PRESTO, Japan Science and Technology Agency, Kawaguchi-shi 332-0012, Japan;* orcid.org/0000-0003-0180-816X; Email: kazu-n@g.ecc.u-tokyo.ac.jp

https://doi.org/10.1021/acssensors.1c02378
ACS Sens. 2022, 7, 534−544

Takeshi Yanagida − *Department of Applied Chemistry, Graduate School of Engineering, The University of Tokyo, Tokyo 113-8656, Japan; Institute for Materials Chemistry and Engineering, Kyushu University, Fukuoka 816-8580, Japan;* orcid.org/0000-0003-4837-5701; Email: yanagida@g.ecc.u-tokyo.ac.jp

Authors

Jiangyang Liu − *Department of Applied Chemistry, Graduate School of Engineering, The University of Tokyo, Tokyo 113-8656, Japan;* orcid.org/0000-0001-5456-7705

Takuro Hosomi − *Department of Applied Chemistry, Graduate School of Engineering, The University of Tokyo, Tokyo 113-8656, Japan; PRESTO, Japan Science and Technology Agency, Kawaguchi-shi 332-0012, Japan;* orcid.org/0000-0002-5649-6696

Wenjin Lei − *Department of Applied Chemistry, Graduate School of Engineering, The University of Tokyo, Tokyo 113-8656, Japan*

Guozhu Zhang − *Department of Applied Chemistry, Graduate School of Engineering, The University of Tokyo, Tokyo 113-8656, Japan*

Tsunaki Takahashi − *Department of Applied Chemistry, Graduate School of Engineering, The University of Tokyo, Tokyo 113-8656, Japan; PRESTO, Japan Science and Technology Agency, Kawaguchi-shi 332-0012, Japan;* orcid.org/0000-0002-2840-8038

Xixi Zhao − *Department of Applied Chemistry, Graduate School of Engineering, The University of Tokyo, Tokyo 113-8656, Japan*

Yosuke Hanai − *Panasonic Corporation, Industrial Solutions Company, Sensing Solutions Development Center, Kadoma 571-8506, Japan*

Atsuo Nakao − *Panasonic Corporation, Industrial Solutions Company, Sensing Solutions Development Center, Kadoma 571-8506, Japan*

Masaya Nakatani − *Panasonic Corporation, Industrial Solutions Company, Sensing Solutions Development Center, Kadoma 571-8506, Japan*

Wataru Tanaka − *Department of Applied Chemistry, Graduate School of Engineering, The University of Tokyo, Tokyo 113-8656, Japan*

Hikaru Saito − *Institute for Materials Chemistry and Engineering, Kyushu University, Fukuoka 816-8580, Japan;* orcid.org/0000-0001-9578-1433

Masaki Kanai − *Institute for Materials Chemistry and Engineering, Kyushu University, Fukuoka 816-8580, Japan*

Taisuke Shimada − *Department of Biomolecular Engineering, Graduate School of Engineering, Nagoya University, Nagoya 464-8603, Japan*

Takao Yasui − *Department of Biomolecular Engineering, Graduate School of Engineering, Nagoya University, Nagoya 464-8603, Japan;* orcid.org/0000-0003-0333-3559

Yoshinobu Baba − *Department of Biomolecular Engineering, Graduate School of Engineering, Nagoya University, Nagoya 464-8603, Japan*

Complete contact information is available at: https://pubs.acs.org/10.1021/acssensors.1c02378

Author Contributions

Sample preparations and characterizations were performed by J.L. and W.L. Device fabrications and sensing measurements of sensors were conducted by J.L., Y.H., A.N., and M.N. K.N. and T.Y. designed this work. The selective water adsorption properties were discussed by J.L., K.N., T.H., G.Z., T.T., X.Z., W.T., M.K., T.S., T.Y., Y.B., and T.Y. T.Y. wrote this manuscript. K.N., T.H., T.T., W.T., and M.K. contributed to improve the manuscript. All authors approved the final version of the manuscript.

Notes

The authors declare no competing financial interest.

■ ACKNOWLEDGMENTS

This work was supported by the JSPS KAKENHI (grant numbers JP18H01831, JP18H05243, JP20H02208, JP21K18868, and JP21K14475), CREST (grant no. JPMJCR19I2), AMED (grant no. JP21zf0127004), the Kurita Water and Environment Foundation, PRESTO (grant no. JPMJPR19J7), the MEXT Project of "Integrated Research Consortium on Chemical Sciences", and the JACI Prize for Encouraging Young Researcher. This work was partly performed under the Cooperative Research Program of "Dynamic Alliance for Open Innovation Bridging Human, Environment and Materials" and the "Network Joint Research Center for Materials and Devices".

■ REFERENCES

(1) Jeong, S. Y.; Kim, J. S.; Lee, J. H. Rational Design of Semiconductor-Based Chemiresistors and Their Libraries for Next-Generation Artificial Olfaction. *Adv. Mater.* **2020**, *32*, 2002075.

(2) Peng, G.; Trock, E.; Haick, H. Detecting Simulated Patterns of Lung Cancer Biomarkers by Random Network of Single-walled Carbon Nanotubes Coated with Nonpolymeric Organic Materials. *Nano Lett.* **2008**, *8*, 3631−3635.

(3) Barsan, N.; Weimar, U. Conduction Model of Metal Oxide Gas Sensors. *J. Electroceram.* **2001**, *7*, 143−167.

(4) Koziej, D.; Bârsan, N.; Weimar, U.; Szuber, J.; Shimanoe, K.; Yamazoe, N. Water−Oxygen Interplay on Tin Dioxide Surface: Implication on Gas Sensing. *Chem. Phys. Lett.* **2005**, *410*, 321−323.

(5) Yamazoe, N.; Fuchigami, J.; Kishikawa, M.; Seiyama, T. Interactions of Tin Oxide Surface with O_2, H_2O and H_2. *Surf. Sci.* **1979**, *86*, 335−344.

(6) Song, Z.; Fan, J.; Shan, Y.; Ng, A. M. C.; Xu, H. Generation of Highly Reactive Oxygen Species on Metal-supported MgO (100) Thin Films. *Phys. Chem. Chem. Phys.* **2016**, *18*, 25373−25379.

(7) Krumova, K.; Cosa, G. Overview of Reactive Oxygen Species. In *Singlet Oxygen: Applications in Biosciences and Nanosciences*; Nonell, S., Flors, C., Eds.; Royal Society of Chemistry: Cambridge, 2016.

(8) Brown, M. E.; de Beurs, K. M.; Marshall, M. Global Phenological Response to Climate Change in Crop Areas Using Satellite Remote Sensing of Vegetation, Humidity and Temperature Over 26 years. *Remote Sens. Environ.* **2012**, *126*, 174−183.

(9) Sunahara, S. *Handbook of Chemical Sensors*; Fiji Techno Systems, 1986; pp 331−342.

(10) Qu, F.; Zhang, S.; Huang, C.; Guo, X.; Zhu, Y.; Thomas, T.; Guo, H.; Attfield, J. P.; Yang, M. Surface Functionalized Sensors for Humidity-Independent Gas Detection. *Angew. Chem., Int. Ed.* **2021**, *60*, 6561−6566.

(11) Yoon, J.-W.; Kim, J.-S.; Kim, T.-H.; Hong, Y. J.; Kang, Y. C.; Lee, J.-H. A New Strategy for Humidity Independent Oxide Chemiresistors: Dynamic Self-refreshing of In_2O_3 Sensing Surface Assisted by Layer-by-layer Coated CeO_2 nanoclusters. *Small* **2016**, *12*, 4229−4240.

(12) Yamazoe, N.; Suematsu, K.; Shimanoe, K. Gas Reception and Signal Transduction of Neat Tin Oxide Semiconductor Sensor for Response to Oxygen. *Thin Solid Films* **2013**, *548*, 695−702.

(13) Farahani, H.; Wagiran, R.; Hamidon, M. Humidity Sensors Principle, Mechanism, and Fabrication Technologies: A comprehensive Review. *Sensors* **2014**, *14*, 7881−7939.

(14) Jung, H. S.; Verwilst, P.; Kim, W. Y.; Kim, J. S. Fluorescent and Colorimetric Sensors for the Detection of Humidity or Water Content. *Chem. Soc. Rev.* **2016**, *45*, 1242−1256.
(15) Cox, D.; Hoflund, G. B.; Laitinen, H. A. A Study of the Dehydration of Tin Oxide Surface Layers. *Appl. Surf. Sci.* **1984**, *20*, 30−38.
(16) Rakow, N. A.; Suslick, K. S. A Colorimetric Sensor Array for Odour Visualization. *Nature* **2000**, *406*, 710−713.
(17) Lee, J.; Seo, S.; Kim, J. Colorimetric Detection of Warfare Gases by Polydiacetylenes Toward Equipment-free Detection. *Adv. Funct. Mater.* **2012**, *22*, 1632−1638.
(18) Courbat, J.; Briand, D.; Damon-Lacoste, J.; Wöllenstein, J.; de Rooij, N. F. Evaluation of pH Indicator-based Colorimetric Films for Ammonia Detection Using Optical Waveguides. *Sens. Actuators, B* **2009**, *143*, 62−70.
(19) Gill, U.; Sutherland, T.; Himbert, S.; Zhu, Y.; Rheinstädter, M. C.; Cranston, E. D.; Moran-Mirabal, J. M.; Jose, M. M. Beyond Buckling: Humidity-independent Measurement of the Mechanical Properties of Green Nanobiocomposite films. *Nanoscale* **2017**, *9*, 7781−7790.
(20) Ma, N.; Suematsu, K.; Yuasa, M.; Shimanoe, K. Pd Size Effect on the Gas Sensing Properties of Pd-loaded SnO_2 in Humid Atmosphere. *ACS Appl. Mater. Interfaces* **2015**, *7*, 15618−15625.
(21) Ma, N.; Suematsu, K.; Yuasa, M.; Kida, T.; Shimanoe, K. Effect of Water Vapor on Pd-loaded SnO_2 Nanoparticles Gas Sensor. *ACS Appl. Mater. Interfaces* **2015**, *7*, 5863−5869.
(22) Choi, K.-I.; Kim, H.-J.; Kang, Y. C.; Lee, J.-H. Ultraselective and Ultrasensitive Detection of H_2S in Highly Humid Atmosphere Using CuO-loaded SnO_2 Hollow Spheres for Real-time Diagnosis of Halitosis. *Sens. Actuators, B* **2014**, *194*, 371−376.
(23) Yang, M.; Lu, J.; Wang, X.; Zhang, H.; Chen, F.; Sun, J.; yang, J.; Sun, Y.; Lu, G. Acetone Sensors with High Stability to Humidity Changes Based on Ru-doped NiO Flower-like Microspheres. *Sens. Actuators, B* **2020**, *313*, 127965.
(24) Choi, K.-I.; Hübner, M.; Haensch, A.; Kim, H.-J.; Weimar, U.; Barsan, N.; Lee, J.-H. Ambivalent Effect of Ni Loading on Gas Sensing Performance in SnO_2 Based Gas Sensor. *Sens. Actuators, B* **2013**, *183*, 401−410.
(25) Kwak, C.-H.; Kim, T.-H.; Jeong, S.-Y.; Yoon, J.-W.; Kim, J.-S.; Lee, J.-H. Humidity-independent Oxide Semiconductor Chemiresistors Using Terbium-doped SnO_2 Yolk−shell Spheres for Real-time Breath Analysis. *ACS Appl. Mater. Interfaces* **2018**, *10*, 18886−18894.
(26) Kim, J.-S.; Na, C. W.; Kwak, C.-H.; Li, H.-Y.; Yoon, J. W.; Kim, J.-H.; Jeong, S.-Y.; Lee, J.-H. Humidity-independent Gas Sensors Using Pr-doped In_2O_3 Macroporous Spheres: Role of Cyclic Pr^{3+}/Pr^{4+} Redox Reactions in Suppression of Water-poisoning Effect. *ACS Appl. Mater. Interfaces* **2019**, *11*, 25322−25329.
(27) Yamazoe, N.; Miura, N. Environmental Gas Sensing. *Sens. Actuators, B* **1994**, *20*, 95−102.
(28) Degler, D.; Weimar, U.; Barsan, N. Current Understanding of the Fundamental Mechanisms of Doped and Loaded Semiconducting Metal-oxide-based Gas Sensing Materials. *ACS Sens.* **2019**, *4*, 2228−2249.
(29) Suematsu, K.; Yuasa, M.; Kida, T.; Yamazoe, N.; Shimanoe, K. Determination of Oxygen Adsorption Species on SnO_2: Exact Analysis of Gas Sensing Properties Using a Sample Gas Pretreatment System. *J. Electrochem. Soc.* **2014**, *161*, B123−B128.
(30) Kawamura, K.; Vestergaard, M. D.; Ishiyama, M.; Nagatani, N.; Hashiba, T.; Tamiya, E. Development of a Novel Hand-held Toluene Gas Sensor: Possible Use in the Prevention and Control of Sick Building Syndrome. *Measurement* **2006**, *39*, 490−496.
(31) Güntner, A. T.; Abegg, S.; Wegner, K.; Pratsinis, S. E. Zeolite Membranes for Highly Selective Formaldehyde Sensors. *Sens. Actuators, B* **2018**, *257*, 916−923.
(32) Van den Broek, J.; Abegg, S.; Pratsinis, S. E.; Güntner, A. T. Highly Selective Detection of Methanol over Ethanol by a Handheld Gas Sensor. *Nat. Commun.* **2019**, *10*, 4220.
(33) Yoon, B.; Choi, S.-J.; Swager, T. M.; Walsh, G. F. Flexible Chemiresistive Cyclohexanone Sensors Based on Single-Walled Carbon Nanotube−Polymer Composites. *ACS Sens.* **2021**, *6*, 3056−3062.
(34) Mahdavi, H.; Rahbarpour, S.; Hosseini-Golgoo, S.-M.; Jamaati, H. Reducing the Destructive Effect of Ambient Humidity Variations on Gas Detection Capability of a Temperature Modulated Gas Sensor by Calcium Chloride. *Sens. Actuators, B* **2021**, *331*, 129091.
(35) Scovazzo, P.; Scovazzo, A. J. Isothermal Dehumidification or Gas Drying Using Vacuum Sweep Dehumidification. *Appl. Therm. Eng.* **2013**, *50*, 225−233.
(36) Ito, D.; Jespersen, M. L.; Hutchison, J. E. Selective Growth of Vertical ZnO Nanowire Arrays Using Chemically Anchored Gold Nanoparticles. *ACS Nano* **2008**, *2*, 2001−2006.
(37) Liu, J.; Nagashima, K.; Nagamatsu, Y.; Hosomi, T.; Saito, H.; Wang, C.; Mizukami, W.; Zhang, G.; Samransuksamer, B.; Takahashi, T.; Kanai, M.; Yasui, T.; Baba, Y.; Yanagida, T. The impact of surface Cu^{2+} of ZnO/$(Cu_{1-x}Zn_x)O$ Heterostructured Nanowires on the Adsorption and Chemical Transformation of Carbonyl Compounds. *Chem. Sci.* **2021**, *12*, 5073−5081.
(38) Wang, C.; Hosomi, T.; Nagashima, K.; Takahashi, T.; Zhang, G.; Kanai, M.; Yoshida, H.; Yanagida, T. Phosphonic Acid Modified ZnO Nanowire Sensors: Directing Reaction Pathway of Volatile Carbonyl Compounds. *ACS Appl. Mater. Interfaces* **2020**, *12*, 44265−44272.
(39) Xu, Q.; Yang, Y.; Yang, J.; Wang, X.; Wang, Z.; Wang, Y. Plasma Activation of Porous Polytetrafluoroethylene Membranes for Superior Hydrophilicity and Separation Performances via Atomic Layer Deposition of TiO_2. *J. Membr. Sci.* **2013**, *443*, 62−68.
(40) Rammelberg, H. U.; Schmidt, T.; Ruck, W. Hydration and Dehydration of Salt Hydrates and Hydroxides for Thermal Energy Storage-kinetics and Energy Release. *Energy Proc.* **2012**, *30*, 362−369.
(41) Molenda, M.; Stengler, J.; Linder, M.; Wörner, A. Reversible Hydration Behavior of $CaCl_2$ at High H_2O Partial Pressures for Thermochemical Energy Storage. *Thermochim. Acta* **2013**, *560*, 76−81.
(42) Aristov, Y. I.; Restuccia, G.; Tokarev, M. M.; Buerger, H.-D.; Freni, A. Selective Water Sorbents for Multiple Applications. 11. $CaCl_2$ Confined to Expanded Vermiculite. *React. Kinet. Catal. Lett.* **2000**, *71*, 377−384.
(43) N'Tsoukpoe, K. E.; Schmidt, T.; Rammelberg, H. U.; Watts, B. A.; Ruck, W. K. L. A Systematic Multi-step Screening of Numerous Salt Hydrates for Low Temperature Thermochemical Energy Storage. *Appl. Energy* **2014**, *124*, 1−16.
(44) Szanyi, J.; Kwak, J. H.; Chimentao, R. J.; Peden, C. H. F. Effect of H_2O on the Adsorption of NO_2 on γ-Al_2O_3: an in situ FTIR/MS Study. *J. Phys. Chem. C* **2007**, *111*, 2661−2669.
(45) Karunadasa, S. Dehydration of Calcium Chloride as Examined by High-temperature X-ray Powder Diffraction. *Int. Multidiscip. Res. J.* **2019**, *4*, 37−43.
(46) Uriarte, L. M.; Dubessy, J.; Boulet, P.; Baonza, V. G.; Bihannic, I.; Robert, P. Reference Raman Spectra of Synthesized $CaCl_2 \cdot nH_2O$ solids (n= 0, 2, 4, 6). *J. Raman Spectrosc.* **2015**, *46*, 822−828.
(47) Wyszynski, B.; Yatabe, R.; Nakao, A.; Nakatani, M.; Oki, A.; Oka, H.; Toko, K. Array of Chemosensitive Resistors with Composites of Gas Chromatography (GC) Materials and Carbon Black for Detection and Recognition of VOCs: A Basic Study. *Sensors* **2017**, *17*, 1606.
(48) Shunori, A.; Yatabe, R.; Wyszynski, B.; Hanai, Y.; Nakao, A.; Nakatani, M.; Oki, A.; Oka, H.; Washio, T.; Toko, K. Multichannel Odor Sensor System using Chemosensitive Resistors and Machine Learning. *2019 IEEE International Symposium on Olfaction and Electronic Nose (ISOEN)*, 2019; pp 1−3.
(49) He, Y.; Yanagida, T.; Nagashima, K.; Zhuge, F.; Meng, G.; Xu, B.; Klamchuen, A.; Rahong, S.; Kanai, M.; Li, X.; Suzuki, M.; Kai, S.; Kawai, T. Crystal-Plane Dependence of Critical Concentration for Nucleation on Hydrothermal ZnO Nanowires. *J. Phys. Chem. C* **2013**, *117*, 1197−1203.
(50) Sakai, D.; Nagashima, K.; Yoshida, H.; Kanai, M.; He, Y.; Zhang, G.; Zhao, X.; Takahashi, T.; Yasui, T.; Hosomi, T.; Uchida, Y.; Takeda, S.; Baba, Y.; Yanagida, T. Substantial Narrowing on the Width of "Concentration Window" of Hydrothermal ZnO Nanowires via Ammonia Addition. *Sci. Rep.* **2019**, *9*, 14160.

https://doi.org/10.1021/acssensors.1c02378
ACS Sens. 2022, 7, 534−544

(51) Akihiro, Y.; Nagashima, K.; Hosomi, T.; Kanai, M.; Anzai, H.; Takahashi, T.; Zhang, G.; Yasui, T.; Baba, Y.; Yanagida, T. Water-Organic Cosolvent Effect on Nucleation of Solution-Synthesized ZnO Nanowires. *ACS Omega* **2019**, *4*, 8299−8304.
(52) Zhao, X.; Nagashima, K.; Zhang, G.; Hosomi, T.; Yoshida, H.; Akihiro, Y.; Kanai, M.; Mizukami, W.; Zhu, Z.; Takahashi, T.; Suzuki, M.; Samransuksamer, B.; Yasui, T.; Aoki, Y.; Baba, Y.; Yanagida, T.; Yanagida, T. Synthesis of Monodispesedly Sized ZnO Nanowires from Randomly Sized Seeds. *Nano Lett.* **2020**, *20*, 599−605.
(53) Liu, J.; Nagashima, K.; Yamashita, H.; Mizukami, W.; Uzuhashi, J.; Hosomi, T.; Kanai, M.; Zhao, X.; Miura, Y.; Zhang, G.; Takahashi, T.; Suzuki, M.; Sakai, D.; Samransuksamer, B.; He, Y.; Ohkubo, T.; Yasui, T.; Aoki, Y.; Ho, J. C.; Baba, Y.; Yanagida, T. Face-selective tungstate ions drive zinc oxide nanowire growth direction and dopant incorporation. *Commun. Mater.* **2020**, *1*, 58.

https://doi.org/10.1021/acssensors.1c02378
ACS Sens. 2022, 7, 534−544